Accuracy Assessment of Non-intrusive Measurement of Two-Port Impedance and Admittance Parameters by Inductive Couplers

Simone Negri
Department of Electronics, Information and Bioengineering
Politecnico di Milano
Milano, Italy
simone.negri@polimi.it

Giordano Spadacini
Department of Electronics, Information and Bioengineering
Politecnico di Milano
Milano, Italy
giordano.spadacini@polimi.it

Flavia Grassi
Department of Electronics, Information and Bioengineering
Politecnico di Milano
Milano, Italy
flavia.grassi@polimi.it

Sergio A. Pignari
Department of Electronics, Information and Bioengineering
Politecnico di Milano
Milano, Italy
sergio.pignari@polimi.it

***Abstract*—Many applications, ranging from power electronics to electromagnetic interference modelling, take advantage of in-circuit impedance and admittance measurements, that is, carried out while equipment is operating. Single-port literature methods, based on the use of clamp-on inductive probes to couple the ports of a vector network analyser (VNA) with the system under test, are advantageous due to their non-intrusive setup, but are not suitable for multiport systems. Just recently, two-port inductively-coupled methods were proposed in two different formulations, namely, for measurement of the full 2×2 admittance and impedance matrix, respectively. In this paper, a comparative investigation on the accuracy provided by the inductively-coupled admittance and impedance measurement methods is presented. Both methods are tested using a suitable set of passive networks in the 150 kHz - 30 MHz frequency range. The obtained results are compared versus an accurate (yet intrusive) reference result, that is, impedance and admittance parameters mathematically converted from scattering parameters directly measured at VNA ports without using inductive couplers. The accuracy of both methods is quantified and discussed, providing useful insights on how to possibly improve the measurement setup.**

Keywords— In-circuit impedance measurement, in-circuit admittance measurement, behavioural models.

I. Introduction

Obtaining frequency responses of single components and complex systems by in-circuit impedance and admittance measurements is of interest for a significant number of different applications, as the non-intrusive nature of inductive probes easily allows the characterization of the equipment under test (EUT) in real operating conditions. Electromagnetic Interference (EMI) modelling particularly benefits from inductively-coupled in-circuit measurements, as inductive probes allow to use sensitive RF instruments on operating power systems, which would not be possible otherwise [1]. Relevant examples include EMI filter design, specifically common mode (CM) [2] and complete EMI [3] filters, and EMI filters performance assessment, considering both single phase [4], [5] and three-phase [6] examples. Additionally, in-circuit measurements can be fruitfully exploited to determine broadband behavioural models of converters, represented as EMI sources [7], [8].

The original concept of inductively coupled in-circuit measurements was based on two inductive probes, hence commonly known as two-probe setup (TPS) [9], and intended for power lines in-circuit impedance measurement [10]. Successively, the TPS was widely used in EMI analysis [3] and for online monitoring of various electrical devices [11], including transformers [12] and photovoltaic PV systems [13]. A simpler setup based on a single inductive probe, commonly known as single-probe setup (SPS) [6], [14], [15] was successfully used to characterize a motor-drive system physical [6] or modal [16], [17] impedances, and recently adapted to time-varying impedance measurements [18] as well. However, both TPS and SPS are not suitable to measure mutual impedances or admittances in multiport systems, which can be represented properly in terms of full matrices only. To address this limitation, an inductively coupled multi-port and multi-probe measurement setup (MPS) proved to be suitable to characterize full 2×2 admittance matrices of passive and active EUTs [19]. Thanks to the choice of admittance (and not impedance) parameters, the behavioural circuit model of the EUT [4], [20] is easily obtained in form of a Norton equivalent circuit, and the MPS and can be extended to any number of ports [21]. Additionally, alternative formulations of the same setup proved to be effective to measure 2×2 modal admittance matrices [22] and 2×2 impedance matrices [23].

In this context, this paper proposes a comparative investigation of the accuracy of the measurement results obtained by the inductively-coupled in-circuit admittance measurement method [19] and by the inductively-coupled in-circuit impedance measurement method [23]. In particular, a number of test networks are directly measured by a VNA, obtaining their reference S-parameters. The latter are then mathematically converted into admittance and impedance parameters, which are used as reference for the two inductively coupled measurement methods. The accuracy of both methods is quantified and discussed, providing useful insights on how to possibly improve each measurement setup.

The paper is structured as follows: Section II and III recall the measurement principle and calibration procedure for the inductively coupled admittance and impedance measurement methods, respectively. Section IV presents the experimental setup used for both methods, while Section V and VI report the measurement results obtained by the two methods. The

This study was carried out within the MOST – Sustainable Mobility Center and received funding from the European Union Next-Generation EU (PIANO NAZIONALE DI RIPRESA E RESILIENZA (PNRR) - MISSIONE 4 COMPONENTE 2, INVESTIMENTO 1.4 - D.D. 1033 17/06/2022, CN00000023). This manuscript reflects only the authors' views and opinions, neither the European Union nor the European Commission can be considered responsible for them.

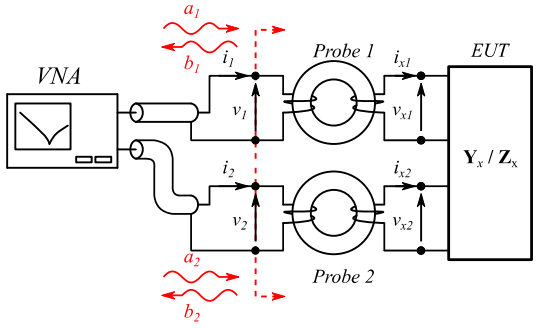

Fig. 1. Principle schematic of the considered two-port setup [19], [23].

accuracy of both methods is discussed in Section VII, while Section VIII reports final conclusions and possible future developments.

II. In-Circuit Measurement of 2×2 Admittance Matrices

A. Measurement Principle

Consider first the setup presented in Fig. 1, which includes a VNA, two inductive probes, and a 2-port EUT. It is desired to determine the EUT 2×2 unknown admittance matrix $\mathbf{Y}_x$ from the knowledge of the S-parameter matrix $\mathbf{S}_m$, representative of the whole setup, directly measured by the VNA. Assuming that the transmission (ABCD) parameters of each probe are known, namely:

$$\begin{bmatrix} v_1 \\ i_1 \end{bmatrix} = \underbrace{\begin{bmatrix} A_1 & B_1 \\ C_1 & D_1 \end{bmatrix}}_{\mathbf{T}_1} \begin{bmatrix} v_{x1} \\ i_{x1} \end{bmatrix}, \quad \begin{bmatrix} v_2 \\ i_2 \end{bmatrix} = \underbrace{\begin{bmatrix} A_2 & B_2 \\ C_2 & D_2 \end{bmatrix}}_{\mathbf{T}_2} \begin{bmatrix} v_{x2} \\ i_{x2} \end{bmatrix}. \tag{1}$$

the entries of the admittance matrix $\mathbf{Y}_x$ can be expressed as a function of the measured S-parameters and of seven complex, frequency-depending constant coefficients k_i [19] as:

$$\begin{aligned} Y_{x11} &= \frac{k_1 + k_2 S_{m11} + k_2 k_7 \det[\mathbf{S}_m] + k_1 k_7 S_{m22}}{1 + k_6 S_{m11} + k_6 k_7 \det[\mathbf{S}_m] + k_7 S_{m22}}, \\ Y_{x12} &= -\frac{k_3 S_{m12}}{1 + k_6 S_{m11} + k_6 k_7 \det[\mathbf{S}_m] + k_7 S_{m22}}, \\ Y_{x21} &= -\frac{k_3 S_{m21}}{1 + k_6 S_{m11} + k_6 k_7 \det[\mathbf{S}_m] + k_7 S_{m22}}, \\ Y_{x22} &= \frac{k_4 + k_4 k_6 S_{m11} + k_5 k_6 \det[\mathbf{S}_m] + k_5 S_{m22}}{1 + k_6 S_{m11} + k_6 k_7 \det[\mathbf{S}_m] + k_7 S_{m22}}. \end{aligned} \tag{2}$$

Coefficients k_1, k_2, k_3, k_4, k_5, k_6, k_7 appearing in (2) are defined as functions of probes transmission parameters and of the S-parameters reference impedance, and their analytical expressions are available in [19]. The eight ABCD parameters, unfortunately, are not generally known. However, it was proven that directly determining the seven coefficients k_i [19] to be used in (2) by an overall calibration procedure is generally faster and easier.

B. Calibration Procedure

While equations (2) are generally fully coupled, it can be observed that, under the hypothesis of uncoupled ports ($S_{m12} = S_{m21} = 0$, hence $Y_{x12} = Y_{x21} = 0$), they can be simplified resulting in separate equations for the self-admittance terms, namely:

$$Y_{x11}\big|_{S_{m12}=S_{m21}=0} = \frac{k_1 + k_2 S_{m11}}{1 + k_6 S_{m11}}, \; Y_{x22}\big|_{S_{m21}=S_{m12}=0} = \frac{k_4 + k_5 S_{m22}}{1 + k_7 S_{m22}}, \tag{3}$$

which noteworthily represent an alternative formulation [19] of the SPS equations [6], [14] at each port. Hence, the same SPS calibration procedure [6], based on three one-port reference loads of known admittances Y_A, Y_B, Y_C, can be used. First, the reflection S-parameters S_{1A}, S_{1B}, S_{1C} are measured by connecting the three test loads, in turn, to probe 1. A linear system in the variables k_1, k_2, k_6 is hence obtained by enforcing the first of (3), which yields one unique solution. Similarly, by measuring the reflection S-parameters S_{2A}, S_{2B}, S_{2C} by connecting the three reference admittances Y_A, Y_B, Y_C, respectively, to probe 2, and enforcing the second of (3), it is possible to obtain a second linear system in the variables k_4, k_5, k_7, which also yields one unique solution.

Lastly, a reference two-port network whose known admittance matrix is denoted as

$$\mathbf{Y}_D = \begin{bmatrix} Y_{D11} & Y_{D12} \\ Y_{D21} & Y_{D22} \end{bmatrix} \tag{4}$$

is required. This reference network is connected to both probes, measuring the full S-parameter matrix

$$\mathbf{S}_D = \begin{bmatrix} S_{D11} & S_{D12} \\ S_{D21} & S_{D22} \end{bmatrix} \tag{5}$$

to determine the last coefficient k_3, which is easily obtained by enforcing data (4), (5) in the mutual admittances (2). The analytical expressions of all coefficients k_i obtained from the calibration procedure are available in [19].

III. In-Circuit Measurement of 2×2 Impedance Matrices

A. Measurement Principle

Consider for a second time the measurement setup reported in Fig. 1, where now the target is to determine the EUT unknown 2×2 impedance matrix $\mathbf{Z}_x$ from the S-parameter matrix $\mathbf{S}_m$ directly measured by the VNA and including the whole setup. The entries of the impedance matrix $\mathbf{Z}_x$ can be expressed as a function of measured S-parameters and of seven complex, frequency-depending constant coefficients h_i [23] as:

$$\begin{aligned} Z_{x11} &= \frac{h_1 + h_2 S_{m11} + h_2 h_7 \det[\mathbf{S}_m] + h_1 h_7 S_{m22}}{1 + h_6 S_{m11} + h_6 h_7 \det[\mathbf{S}_m] + h_7 S_{m22}}, \\ Z_{x12} &= \frac{h_3 S_{m12}}{1 + h_6 S_{m11} + h_6 h_7 \det[\mathbf{S}_m] + h_7 S_{m22}}, \\ Z_{x21} &= \frac{h_3 S_{m21}}{1 + h_6 S_{m11} + h_6 h_7 \det[\mathbf{S}_m] + h_7 S_{m22}}, \\ Z_{x22} &= \frac{h_4 + h_4 h_6 S_{m11} + h_5 h_6 \det[\mathbf{S}_m] + h_5 S_{m22}}{1 + h_6 S_{m11} + h_6 h_7 \det[\mathbf{S}_m] + h_7 S_{m22}}. \end{aligned} \tag{6}$$

Coefficients h_1, h_2, h_3, h_4, h_5, h_5, h_6, h_7 in (6) are defined as functions of probes transmission parameters and of the S-parameters reference impedance, and their analytical expressions are available in [23]. Note that even though the admittance parameters (2) and the impedance parameters (6) are formally similar, the seven coefficients h_i and k_i are totally different. As discussed for the admittance representation in Section II.A, the knowledge of the eight ABCD parameters representing the two probes is practically not needed, as the seven coefficients h_i are directly obtained from an overall calibration procedure [23] and directly used in (6).

B. Calibration Procedure

Similarly to what has been presented in Section II.B, equations (6) degenerate into separate equations if the two ports of the EUT are uncoupled ($S_{m12} = S_{m21} = 0$, and, obviously, $Z_{x12} = Z_{x21} = 0$). In this case, self-impedances can be expressed as:

$$Z_{x11}\big|_{S_{m12}=S_{m21}=0} = \frac{h_1 + h_2 S_{m11}}{1 + h_6 S_{m11}},\ Z_{x22}\big|_{S_{m12}=S_{m21}=0} = \frac{h_4 + h_5 S_{m22}}{1 + h_7 S_{m22}}. \tag{7}$$

Similarly to (3), also the expressions in (7) represent an alternative formulation [23] of the SPS [6], [15]. Hence, the SPS calibration procedure [6] can be used, as proposed in [23]. This procedure is based on three tests on reference loads with known impedances Z_A, Z_B, Z_C. Each load is connected, in turn, to probe 1, to measure the reflection S-parameters S_{1A}, S_{1B}, S_{1C} by the VNA. By enforcing the first of (7), a linear system of three equations in the variables h_1, h_2, h_6 is obtained, the solution of which is unique. Similarly, each load is connected, in turn, to probe 2, to measure the reflection S-parameters S_{2A}, S_{2B}, S_{2C} by the VNA, and, by enforcing the second of (7), a second linear system in the variables h_4, h_5, h_7 is obtained.

Lastly, a reference two-port network with known impedance matrix

$$\mathbf{Z}_D = \begin{bmatrix} Z_{D11} & Z_{D12} \\ Z_{D21} & Z_{D22} \end{bmatrix} \tag{8}$$

is required. This reference network is connected to both probes to determine the last coefficient h_3, which determined by enforcing data (8), (5) in the mutual impedances (6). The analytical expressions of all coefficients h_i obtained from the calibration procedure are available in [23].

IV. Experimental Setup

An experimental setup was realized, according to Fig. 1, for this study, including two inductive probes (BCI probe FCC F-120-2 - probe 1, monitor probe Solar 9123-1N - probe 2) and a Keysight E5061B VNA. Probe 1 and 2 were clamped on two turns and six turns of wire, respectively, to optimize measurement sensitivity [6]. A depiction of the considered setup is reported in Fig. 2, while details on probe selection criteria are available in [19], [23]. For all tests, the VNA measures 1601 points in the frequency range 150 kHz - 30 MHz, with 8 dBm forward power and 100 Hz resolution bandwidth, and a preliminary calibration to account for coaxial cables was performed. A number of measurements were performed on a test network (Fig. 2(a), with $R_1 = 0\ \Omega$, $R_2 = 125\ \Omega$), used with a resistive (50 Ω) or inductive (10 μH) termination to provide different impedance/admittance values. The test network is enclosed in a metallic box equipped with SMA connectors, so that a VNA can be directly connected to measure the reference S-parameters. The latter can be mathematically converted into admittances or impedance parameters to be used as reference values for the inductively coupled admittance and impedance methods, respectively. As shown in Fig. 2(b), the connection between probes and test networks is realized by a couple of short twisted-wire pairs. To allow for embedding their contribution to the reference impedance and admittance values, the two twisted wire pairs were separately characterized and modelled in terms of lumped capacitance and inductance.

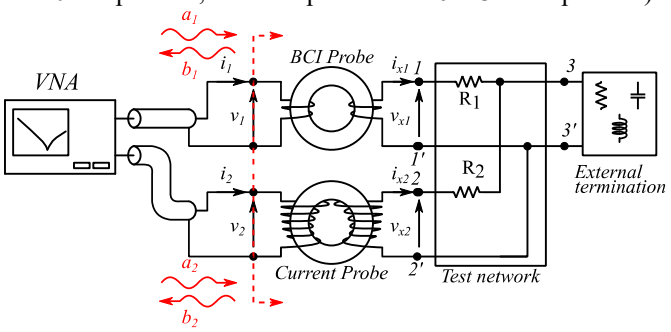

(a)

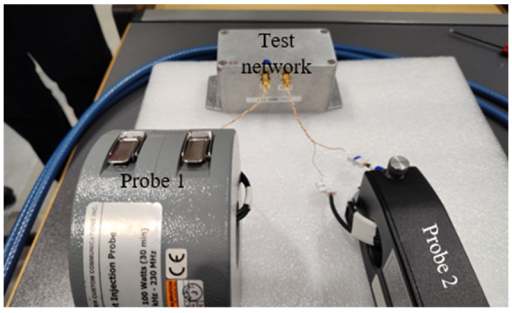

(b)

Fig. 2. Principle representation of the experimental setup for experimental tests [19], [23] (a), and its practical realization (b).

V. Characterization of Two-Port Admittance Parameters

A. Calibration for Admittance Measurements

The calibration procedure relies on four reference resistors (nominal resistances $R_A = 1.1\ \Omega$, $R_B = 50\ \Omega$, $R_C = 1\ \text{k}\Omega$, $R_D = 220\ \Omega$), the admittances Y_A, Y_B, Y_C, Y_D of which are independently determined by an impedance analyser through reflectometric measurements. Successively, each probe is subject to the one-port calibration procedure discussed in [19], based on single impedance measurements (Fig. 3(a)). Lastly, a two-port calibration procedure is performed, which requires a known two port network. This is achieved by connecting the secondary winding of each probe according to Fig. 3(b), with the series connection of the reference load Y_D, resulting in an admittance matrix (4) where $Y_{D11} = Y_{D22} = Y_D$, $Y_{D12} = Y_{D21} = -Y_D$. The coefficients k_1, k_2, k_3, k_4, k_5, k_6, k_7 are hence calculate as discussed in [19].

B. Admittance Measurements Results

Figs. 4 and 5 show the comparison between the admittance parameters of the considered test network with resistive and inductive termination, respectively, resulting from the considered in-circuit measurement method, and their reference values, in magnitude and angle. Accuracy appears to be good over the frequency range of interest, and the variable frequency response of phases is well captured.

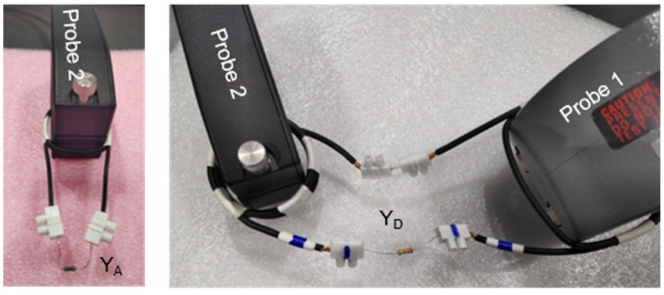

(a) (b)

Fig. 3. (a) One-port calibration setup with monitor probe, and (b) two-port calibration setup.

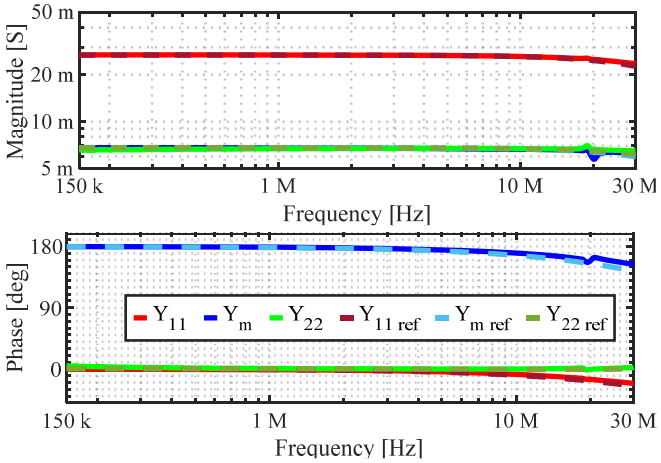

Fig. 4. Admittance matrix entries Y_{11} (red), Y_m (blue), Y_{22} (green) of the test network with resistive termination: comparison between reference (dashed lines) and measured (solid lines) values.

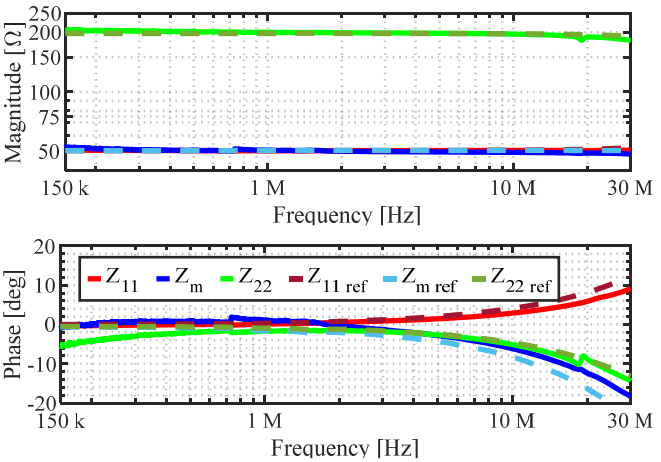

Fig. 7. Impedance matrix entries Z_{11} (red), Z_m (blue), Z_{22} (green) of the test network with resistive termination: comparison between reference (dashed lines) and measured (solid lines) values.

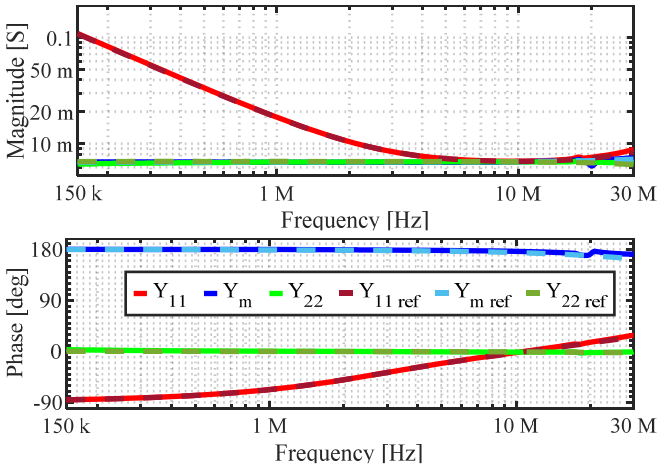

Fig. 5. Admittance matrix entries Y_{11} (red), Y_m (blue), Y_{22} (green) of the test network with inductive termination: comparison between reference (dashed lines) and measured (solid lines) values.

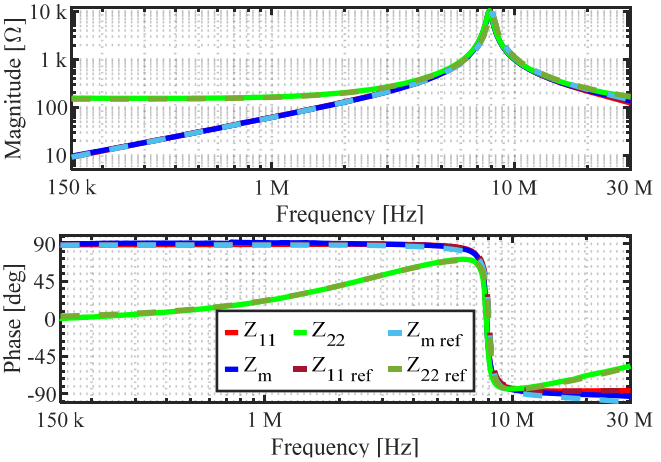

Fig. 8. Impedance matrix entries Z_{11} (red), Z_m (blue), Z_{22} (green) of the test network with inductive termination: comparison between reference (dashed lines) and measured (solid lines) values.

VI. Characterization of Two-Port Impedance Parameters

A. Calibration for Impedance Measurements

The impedance measurement setup calibration procedure also relies on four reference resistors (nominal resistances R_A = 1.1 Ω, R_B = 50 Ω, R_C = 1 kΩ, R_D = 220 Ω, same four resistors used in Section V.A for consistency), the impedances Z_A, Z_B, Z_C, Z_D of which are independently determined by an impedance analyser through reflectometric measurements. Firstly, the three one-port measurements (Fig. 6(a)) required by the calibration procedure [23] are performed. The required two-port measurement is then realized as shown in Fig. 6(b),

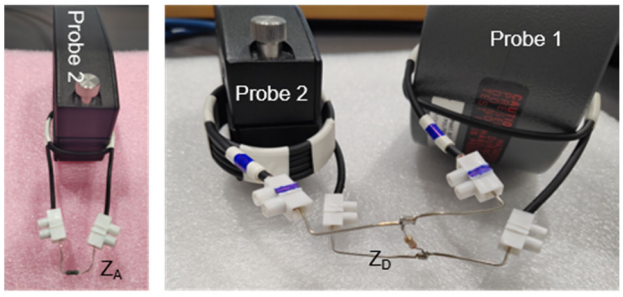

(a) (b)

Fig. 6. (a) One-port calibration setup with BCI probe, and (b) two-port calibration setup.

where the reference load Z_D is connected to both probes secondary windings, resulting in an impedance matrix (8) where $Z_{D11} = Z_{D12} = Z_{D21} = Z_{D22} = Z_D$. The coefficients h_1, h_2, h_3, h_4, h_5, h_6, h_7 are hence calculate as discussed in [23].

B. Impedance Measurements Results

The impedance parameters obtained by the proposed in-circuit measurement method for the resistive and inductive cases, respectively, are compared with their reference values, obtained by direct VNA measurement, in Figs. 7 and 8, in magnitude and angle. Over the whole frequency range of interest, a dynamic range spanning four order of magnitudes is observed, along with good accuracy. In both cases, the frequency-dependent behaviour of impedance angles is well captured.

VII. Accuracy Assessment of Two-Port Admittance and Impedance Measurement Methods

A. Admittance Measurements Accuracy Assessment

The errors between reference admittance values and admittance values obtained by the inductively-coupled admittance impedance method are reported in Figs. 9 and 10 for the resistive termination and inductive termination cases, respectively. Additionally, Table I reports the main error estimators evaluated for the measurements corresponding to Figs. 4 and 5, namely maximum error, average error, and standard deviation.

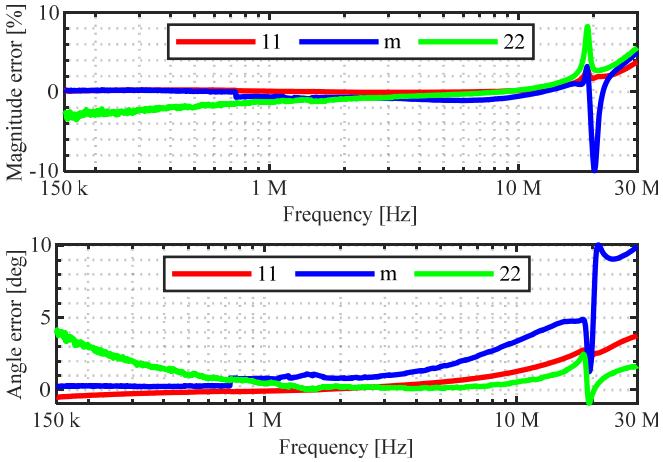

Fig. 9. Relative magnitude and phase deviation between reference values and measured admittance values of the test network with resistive termination.

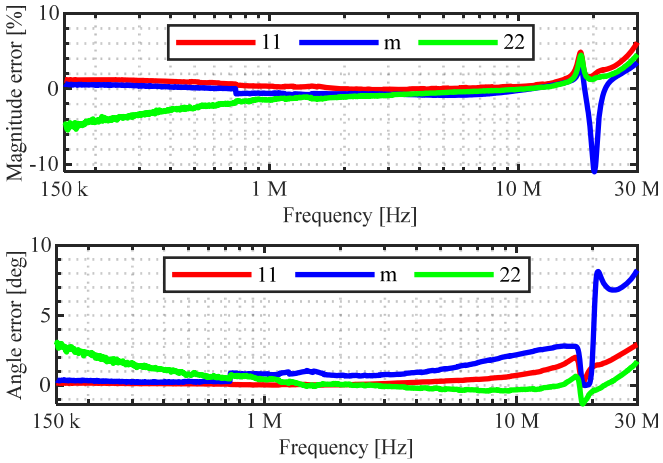

Fig. 10. Relative magnitude and phase deviation between reference values and measured admittance values of the test network with inductive termination.

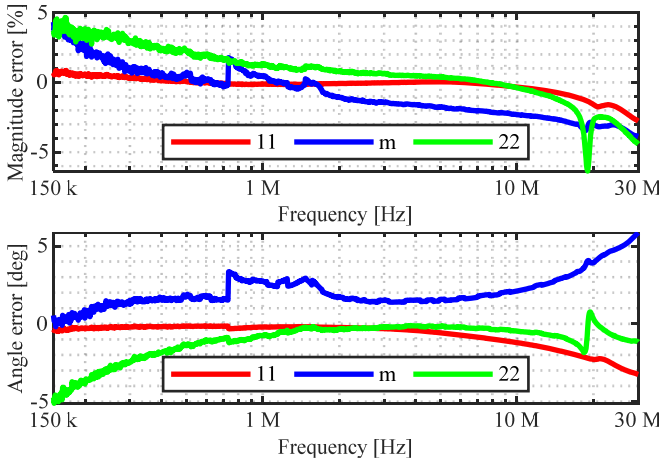

Fig. 11. Relative magnitude and phase deviation between reference values and measured impedance values of the test network with resistive termination.

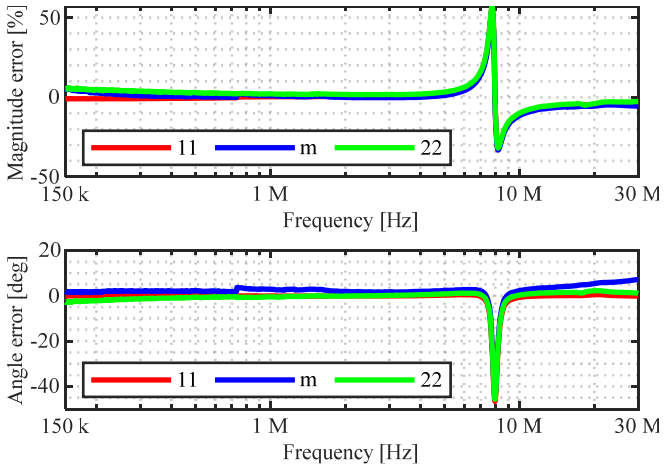

Fig. 12. Relative magnitude and phase deviation between reference values and measured impedance values of the test network with inductive termination.

It can be observed that the magnitude error is constantly smaller than 5% and the angle error smaller than 4 degrees from 150 kHz up to 10 MHz. Only between 10 MHz and 30 MHz, where small resonances in the frequency responses can be observed, the magnitude and angle error reach values up to 10% and 8 degrees, respectively. Additionally, it is possible to observe that the self-admittance measured from port 2 is the only entry showing a non-negligible error at low frequency too (5% mag., 4° angle), which is expected as the monitor probe used for port 2 has six internal turns, which required to use an external six-turns winding to compensate. While the concept of using an external winding with a number of turns equal to the probe internal ones to optimize measurement sensitivity [6] proved to be effective in allowing the use of a variety of probes for admittance/impedance measurements, from Figs. 9 – 12 it appears that the performance of the setup with a monitor probe and a six-turn external winding is inferior to the one obtained from a BCI probe with two internal turns. A possible cause for this reduced performance may be ascribed to the external winding realization, which introduces additional parasitics and geometrical uncertainties, as the winding itself and its relative position with respect to the probe are not perfectly consistent from one test to another. As a consequence, it can be inferred that, if possible, choosing probes with the smallest number of internal turns leads to the best accuracy.

B. Impedance Measurements Accuracy Assessment

The errors between reference impedance values and impedance values obtained by the inductively-coupled impedance method are reported in Figs. 11 and 12 for the resistive termination and inductive termination cases, respectively. Additionally, Table II reports the main error estimators, for the measurements corresponding to Figs. 7, 8.

TABLE I
OVERVIEW OF MAXIMUM AND AVERAGE MEASUREMENT ERRORS IN ADMITTANCE MEASUREMENTS

Case	Par.	Max Mag. Error	Max Angle Error	Avg. Mag. Error	Avg. Angle Error	Mag. Std. Dev.	Phase Std. Dev.
Y, R	Y_{11}	3.8 %	3.8 °	0.38 %	0.58 °	0.70 %	1.4 °
	Y_{22}	8.3 %	4.2 °	-0.50 %	0.94 °	3.9 %	1.8 °
	Y_m	10 %	10 °	-0.24 %	2.0 °	2.0 %	10 °
Y, L	Y_{11}	6.2 %	2.9 °	0.83 %	0.44 °	1.8 %	0.57 °
	Y_{22}	5.4 %	3.1 °	-1.1 %	0.44 °	4.7 %	0.91 °
	Y_m	11 %	8.2 °	-0.22 %	1.4 °	2.0 %	5.5 °

TABLE II
OVERVIEW OF MAXIMUM AND AVERAGE MEASUREMENT ERRORS IN IMPEDANCE MEASUREMENTS

Case	Par.	Max Mag. Error	Max Angle Error	Avg. Mag. Error	Avg. Angle Error	Mag. Std. Dev.	Phase Std. Dev.
Z, R	Z_{11}	2.8 %	3.3 °	-0.22 %	-0.72 °	0.47 %	1.1 °
	Z_{22}	6.4 %	5.1 °	0.70 %	-1.1 °	4.2 %	2.4 °
	Z_m	4.3 %	5.9 °	-0.74 %	2.1 °	3.8 %	5.6 °
Z, L	Z_{11}	56 %	47 °	-0.57 %	-0.67 °	60 %	19 °
	Z_{22}	57 %	46 °	1.4 %	-0.68 °	65 %	19 °
	Z_m	54 %	44 °	-0.47 %	2.1 °	61 %	25 °

It can be observed that the magnitude error is constantly smaller than 10 % and the angle error smaller than 5 degrees from 150 kHz up to 10 MHz. Not dissimilarly from the admittance measurements in Section VII.A, between 10 MHz and 30 MHz the magnitude and angle error increase up to 6.5 % and 6 degrees, respectively. However, for the impedance measurements, a much larger error (50% mag., 50 ° angle) appears around 8 MHz, in correspondence of the resonance of the test network. While this error drives up the error estimators significantly, it can be ascribed to a small deviation in the resonance frequency of the measured impedances with respect to the real one, so that it does not detract significantly from the method effectiveness. Lastly, it is possible to observe that, as for the admittance parameters discussed in Section VII.A, the self-impedance measured from port 2 and the mutual impedance show a non-negligible error at low frequency too (5 % mag., 5 ° angle), while the self-impedance measured from port one does not. This is again ascribed to use of a monitor probe for port 2, which required a six-turn external winding to have acceptable sensitivity.

VIII. CONCLUSION

In this paper, a comparative investigation on the accuracy provided by the inductively-coupled admittance and impedance measurement methods is presented. Both methods are tested by characterizing a set of passive networks in the 150 kHz - 30 MHz frequency range, and comparing measurement results from the considered non-intrusive measurements methods with results obtained by direct VNA measurement.

The accuracy of both methods proved to be good, with comparable error levels, quantified as smaller than 5% in magnitude and 5° in phase in most of the frequency range of interest, with a small increase in the 10 MHz – 30 MHz frequency range. The impedance measurement method showed to slightly misrepresent the resonance frequency of one of the test networks, resulting in large error in a narrow frequency range around the resonance frequency. Further investigation will address this issue, in order to understand if it is specific to the impedance measurement method, or if it can affect also the impedance one under certain circumstances. Additionally, the accuracy assessment showed that the result from the monitor probe used on port 2 suffer from reduced accuracy, especially at low frequency, with respect to the ones obtained from the BCI probe used on port one. Further investigation will be addressed to quantify the impact of probes characteristics on measurement accuracy.

IX. REFERENCES

[1] Z. Zhao et al., “Voltage-dependent capacitance extraction of SiC power MOSFETs using inductively coupled in-circuit impedance measurement technique,” *IEEE Trans. Electromagn. Compat.*, vol. 61, no. 4, pp. 1322–1328, Aug. 2019.

[2] F. Fan, K. Y. See, X. Liu, K. Li and A. K. Gupta, "Systematic Common-Mode Filter Design for Inverter-Driven Motor System Based on In-Circuit Impedance Extraction," in *IEEE IEEE Trans. Electromagn. Compat.*, vol. 62, no. 5, pp. 1711-1722, Oct. 2020.

[3] V. Tarateeraseth, K. Y. See, F. G. Canavero, and R.W.-Y. Chang, “Systematic electromagnetic interference filter design based on information from in-circuit impedance measurements,” *IEEE Trans. Electromagn. Compat.*, vol. 52, no. 3, pp. 588–598, Aug. 2010.

[4] S. Negri, G. Spadacini, F. Grassi and S. A. Pignari, "Black-Box Modeling of EMI Filters for Frequency and Time-Domain Simulations," in *IEEE Trans. Electromagn. Compat.*, vol. 64, no. 1, pp. 119-128, Feb. 2022.

[5] S. Negri, G. Spadacini, F. Grassi and S. A. Pignari, "Prediction of EMI Filter Attenuation in Power-Electronic Converters via Circuit Simulation," in *IEEE Trans. Electromagn. Compat.*, vol. 64, no. 4, pp. 1086-1096, Aug. 2022.

[6] L. Wan, S. Negri, G. Spadacini, F. Grassi, and S. A. Pignari, “Enhanced Impedance Measurement to Predict Electromagnetic Interference Attenuation Provided by EMI Filters in Systems with AC/DC Converters,” *Applied Sciences*, vol. 12, no. 23, p. 12497, Dec. 2022.

[7] A. C. Baisden, D. Boroyevich, and W. Fei, “Generalized terminal modeling of electromagnetic interference,” *IEEE Trans. Ind. Appl.*, vol. 46, no. 5, pp. 2068–2079, Sep./Oct. 2010.

[8] H. Bishnoi, A. C. Baisden, P. Mattavelli and D. Boroyevich, "Analysis of EMI Terminal Modeling of Switched Power Converters," in *IEEE Trans. on Power Electron.,* vol. 27, no. 9, pp. 3924-3933, Sept. 2012.

[9] K. R. Li, K. Y. See, and X. M. Li, “Inductive coupled in-circuit impedance monitoring of electrical system using two-port ABCD network approach,” *IEEE Trans. Instrum. Meas.,* vol. 64, no. 9, pp. 2489–2495, Sep. 2015.

[10] R. A. Southwick and W. C. Dolle, “Line impedance measuring instrumentation utilizing current probe coupling,” *IEEE Trans. Electromagn. Compat.*, vol. 13, no. 4, pp. 31–36, Nov. 1971.

[11] S. B. Rathnayaka *et al.*, “Inductively coupled on-line impedance measurement for condition monitoring of electrical equipment,” *IET Sci., Meas. Tech.,* vol. 12, no. 3, pp. 382–387, May 2018.

[12] S. B. Rathnayaka, K. Y. See, and K. Li, “Online impedance monitoring of transformer based on inductive coupling approach,” *IEEE Trans. Dielectrics Elect. Insul.*, vol. 24, no. 2, pp. 1273–1279, Apr. 2017.

[13] M. Prajapati, F. Fan, Z. Zhao, and K. Y. See, “Estimation of radiated emissions from PV system through black box approach,” *IEEE Trans. Instrum. Meas.*, vol. 70, 2021, Art. no. 9004304.

[14] V.Tarateeraseth, B. Hu, K.Y. See, and F. G. Canavero, “Accurate extraction of noise source impedance of an SMPS under operating conditions,” *IEEE Trans. Power Electron.,* vol. 25, no. 1, pp. 111–117, Jan. 2010.

[15] A. Weerasinghe, Z. Zhao, N. B. Narampanawe, Z. Yang, T. Svimonishvili, and K. Y. See, “Single-probe inductively coupled in-circuit impedance measurement,” *IEEE Trans. Electromagn. Compat.*, vol. 64, no. 1, pp. 2–10, Feb. 2022.

[16] A. Weerasinghe, Z. Zhao, F. Fan, P. Tu and K. Y. See, "In-Circuit Differential-Mode Impedance Extraction at the AC Input of a Motor Drive System," *2021 Asia-Pacific International Symposium on Electromagnetic Compatibility (APEMC)*, Nusa Dua - Bali, Indonesia, 2021, pp. 1-4.

[17] Z. Zhao, F. Fan, A. Weerasinghe, P. Tu and K. Y. See, "Measurement of In-Circuit Common-Mode Impedance at the AC Input of a Motor Drive System," *2021 Asia-Pacific International Symposium on Electromagnetic Compatibility (APEMC)*, Nusa Dua - Bali, Indonesia, 2021, pp. 1-4.

[18] A. Weerasinghe *et al*., "A Novel Single-Probe Setup for Multifrequency Simultaneous Measurement of In-Circuit Impedance," in *IEEE Trans. Ind. Electron.*, vol. 70, no. 9, pp. 9538-9549, Sept. 2023.

[19] S. Negri, G. Spadacini, F. Grassi and S. A. Pignari, "Inductively Coupled in-Circuit Measurement of Two-Port Admittance Parameters," in *IEEE Transactions on Industrial Electronics.* doi: 10.1109/TIE.2024.3357888

[20] S. Negri, G. Spadacini, F. Grassi and S. Pignari, "Measurement-Based Equivalent Circuit Model for Time-Domain Simulation of EMI Filters," *2022 International Symposium on Electromagnetic Compatibility – EMC Europe*, Gothenburg, Sweden, 2022, pp. 793-798.

[21] S. Negri, G. Spadacini, F. Grassi and S. A. Pignari, “Inductively Coupled In-Circuit Measurement of Multiport Admittance Parameters,” in *URSI Radio Science Letters*, Volume 6, 2024.

[22] S. Negri, G. Spadacini, F. Grassi and S. A. Pignari, “Full Modal-Admittance Matrix In-Circuit Measurement by Multiple Inductive Probes,” accepted for presentation at EMC + SIPI 2024.

[23] S. Negri, G. Spadacini, F. Grassi and S. A. Pignari, “Non-intrusive Measurement of Two-Port Impedance Parameters by Clamp-on Inductive Probes,” accepted for presentation at EEEIC 2024.